10

Higher Rank Tensors in Diffusion MRI

Evren Özarslan[1,2], Baba C. Vemuri[2,3], and Thomas H. Mareci[1,2,4]

[1] Department of Physics, University of Florida, Gainesville, FL32611, USA
[2] McKnight Brain Institute, University of Florida, Gainesville, FL32610, USA
[3] Department of Computer and Information Science and Engineering, University of Florida, Gainesville, FL32611, USA
[4] Department of Biochemistry and Molecular Biology, University of Florida, Gainesville, FL32610, USA
evren@mbi.ufl.edu, vemuri@cise.ufl.edu

Summary. In this work we review how the diffusivity profiles obtained from diffusion MRI can be expressed in terms of Cartesian tensors of ranks higher than 2. When the rank of the tensor being used is 2, one recovers traditional diffusion tensor imaging (DTI). Therefore our approach can be seen as a generalization of DTI. The properties of generalized diffusion tensors are discussed. The shortcomings of DTI experienced in the presence of orientational heterogeneity may cause inaccurate anisotropy values and incorrect fiber orientations. Employment of higher rank tensors is helpful in overcoming these difficulties.

10.1 Introduction

The dependence of the magnetic resonance signal intensity on the direction of the applied diffusion sensitizing gradients has been exploited to calculate the local orientations in fibrous tissues, which may eventually lead to the construction of anatomical connections within different regions of the brain. The most common approach used to model orientational dependence of the diffusivities, called diffusion tensor MRI or diffusion tensor imaging (DTI) [1, 2], has employed a Cartesian tensor of rank-2 that has yielded a simple scheme to calculate anisotropy values as well as local orientations of the fibers from multidirectional diffusion measurements. However, the underlying assumption of DTI, i.e. the orientational homogeneity within the voxels, may be too restrictive for the imaging of neural tissue. The incapability of DTI to resolve more than one fiber orientation has prompted recent interest in the development of more sophisticated techniques. A review of DTI along with some of the techniques developed to overcome the failure of DTI in regions of tissue with complex microstructure by Alexander can be found in Chap. 5. Also note that a recent method by Pasternak et al. based on modeling the signal in a variational framework using multiple rank-2 tensors is detailed in the

preceding chapter. In this chapter, we present a technique that we have recently introduced called generalized diffusion tensor imaging that uses tensors of rank possibly higher than 2.

10.1.1 Background

The dynamics of magnetization within the tissue is governed by the Bloch-Torrey equation [3], which, upon simplification to keep its diffusion related parts, takes the form

$$\frac{\partial \psi}{\partial t} = -i\gamma \mathbf{r} \cdot \mathbf{G}\psi + D\nabla^2 \psi \,, \tag{10.1}$$

where $\mathbf{r}$ is the position vector, γ is the gyromagnetic ratio, D is the apparent diffusion coefficient and $\mathbf{G}$ is the linear magnetic field gradient, whose direction $\mathbf{g}$ is assumed to be time independent. In the above expression $\psi := M_+ \exp(iw_0 t + t/T_2)$, where w_0 is the Larmor frequency, T_2 is the spin-spin relaxation constant and M_+ is the complex representation for local transverse magnetization. Integral of M_+ over the voxel yields the signal S received from that voxel. The components of $\mathbf{g}$ can be written in terms of the spherical coordinates as

$$\mathbf{g} := \frac{\mathbf{G}}{||\mathbf{G}||} = \begin{pmatrix} g_1 \\ g_2 \\ g_3 \end{pmatrix} = \begin{pmatrix} \sin\theta\, \cos\phi \\ \sin\theta\, \sin\phi \\ \cos\theta \end{pmatrix} \,, \tag{10.2}$$

where θ is the polar and ϕ is the azimuthal angle.

The solution to (10.1) yields the well known Stejskal-Tanner equation [4], that relates the applied diffusion gradient to the MR signal, given by

$$S(\mathbf{g}) = S_0 \exp(-\gamma^2 \delta^2 ||\mathbf{G}||^2 (\Delta - \delta/3) D(\mathbf{g})) = S_0 \exp(-b\, D(\mathbf{g})) \,, \tag{10.3}$$

where δ is the duration of the gradient pulses and Δ is the time difference between the leading edges of these pulses.

In DTI, one replaces the diffusivity in (10.1) with a rank-2 symmetric positive definite tensor, which results in an approximate signal attenuation expression given by

$$S(\mathbf{g}) = S_0 \exp(-b\, \mathbf{g}^{\mathrm{T}} \mathsf{D} \mathbf{g}) \,. \tag{10.4}$$

Comparison of the last two equations indicates that DTI assumes a diffusivity profile that is specified by the quadratic forms of the rank-2 tensor, i.e.,

$$D(\mathbf{g}) = \mathbf{g}^{\mathrm{T}} \mathsf{D} \mathbf{g} \,. \tag{10.5}$$

10.1.2 Generalized Diffusion Tensor Imaging

As an extension of the transition from a diffusion coefficient (a rank-0 tensor) to the rank-2 diffusion tensor, we have proposed to use Cartesian tensors of rank higher than 2 to model the orientational dependence of diffusivities [5]. In this scheme, generalization of (10.4) is given by

$$S = S_0 \exp\left(-b \sum_{\mathrm{i}_1=1}^{3} \sum_{\mathrm{i}_2=1}^{3} \cdots \sum_{\mathrm{i}_l=1}^{3} D_{\mathrm{i}_1\mathrm{i}_2\ldots\mathrm{i}_l} g_{\mathrm{i}_1} g_{\mathrm{i}_2} \cdots g_{\mathrm{i}_l}\right) , \tag{10.6}$$

where $D_{\mathrm{i}_1\mathrm{i}_2\ldots\mathrm{i}_l}$ represents the components of the rank-l tensor. In this case, the diffusivity profile implied by the rank-l tensor can be expressed as

$$D(\mathbf{g}) = \sum_{\mathrm{i}_1=1}^{3} \sum_{\mathrm{i}_2=1}^{3} \cdots \sum_{\mathrm{i}_l=1}^{3} D_{\mathrm{i}_1\mathrm{i}_2\ldots\mathrm{i}_l} g_{\mathrm{i}_1} g_{\mathrm{i}_2} \cdots g_{\mathrm{i}_l} \ . \tag{10.7}$$

Note that (10.7) implies that

$$D(-\mathbf{g}) = \begin{cases} D(\mathbf{g}), & \text{if } l \text{ is even} \\ -D(\mathbf{g}), & \text{if } l \text{ is odd} \end{cases} . \tag{10.8}$$

However, the latter case would yield negative diffusivities which are nonphysical. Therefore, the rank of the tensor model has te be even in which case antipodal symmetry of the diffusivities is also ensured. Furthermore, (10.7) also implies that the rank-l tensor is a totally symmetric tensor, i.e.,

$$D_{\mathrm{i}_1\mathrm{i}_2\ldots\mathrm{i}_l} = D_{(\mathrm{i}_1\mathrm{i}_2\ldots\mathrm{i}_l)} , \tag{10.9}$$

where $(\mathrm{i}_1\mathrm{i}_2\ldots\mathrm{i}_l)$ stands for all permutations of the indices. This is because the rank-l tensor links the components of the same l vectors to a scalar, therefore the order of these vectors do not affect the result. A totally symmetric tensor in three dimensional space has

$$N_l := \binom{l+2}{2} = \frac{(l+1)(l+2)}{2} \tag{10.10}$$

distinct components [6], where each of these distinct elements is repeated

$$\mu := \binom{l}{n_\mathrm{x}} \binom{l-n_\mathrm{x}}{n_\mathrm{y}} = \frac{l!}{n_\mathrm{x}!\, n_\mathrm{y}!\, n_\mathrm{z}!} \tag{10.11}$$

times[1], where n_x, n_y and n_z are respectively the number of x, y and z indices included in the full sequence of subscripts defining the component of

[1] Note that the properties of the higher order diffusion tensor as described in the text follows from the expression given in (10.7). A similar expression is found in the linear theory of elasticity where the elastic energy U (a scalar) is obtained

the tensor. For example, for D_{xxxz}, i.e., xxxz component of the rank-4 tensor, $n_{\mathrm{x}} = 3$, $n_{\mathrm{y}} = 0$ and $n_{\mathrm{z}} = 1$. Therefore, using (10.11), it is easy to see that the multiplicity, μ, of this component is 4.

These findings can be incorporated into (10.6) to yield a simplified expression for the generalized Stejskal-Tanner equation:

$$S = S_0 \exp\left(-b \sum_{\mathrm{k}=1}^{N_{\mathrm{l}}} \mu_{\mathrm{k}} D_{\mathrm{k}} \prod_{\mathrm{p}=1}^{\mathrm{l}} g_{\mathrm{k(p)}}\right) , \tag{10.12}$$

where D_{k} is the k-th distinct element of the tensor, and $g_{\mathrm{k(p)}}$ is the component of the gradient direction specified by the p-th index of D_{k}.

A rank-l tensor contains the information stored in tensors of rank smaller than l. Therefore, once a rank-l tensor is calculated, the components of the lower rank tensors can be derived from this rank-l tensor. For example the rank-0 tensor has only 1 component and is given in terms of the components of the rank-2 tensor by $D = 1/3(D_{\mathrm{xx}} + D_{\mathrm{yy}} + D_{\mathrm{zz}})$. The derivations of these relations involve using the irreducible representation of the tensor and are given in [5].

10.2 Quantification of Anisotropy from Higher Rank Tensors

One of the most widely utilized achievements of DTI has been the parametrization of anisotropy, which produces a new contrast mechanism between highly structured tissue and others[2]. It has been found in numerous studies that changes in the neural tissue integrity due to many pathologies are reflected on the values obtained from anisotropy maps [7]. Many indices have been proposed to date that relate the observed signal intensities to an anisotropy value. Most of these formulations are based upon the rank-2 tensor model of DTI. In Chap. 17, Moakher and Batchelor present a new approach to the quantification of anisotropy from rank-2 diffusion tensors. However, the failure of DTI in the presence of orientational heterogeneity introduces a major problem in the anisotropy values calculated. This is because when there is more than one orientation within the voxel of interest, using the rank-2 tensor model gives rise

from the elasticity tensor E (a rank-4 tensor) through the relationship

$$U = \frac{1}{2} E_{ijkl}\, \zeta_{ij}\, \zeta_{kl} \ .$$

The differences in the properties of the elasticity tensor when compared to the rank-4 diffusion tensor stem from the fact that the former links the components of the strain tensor ζ (a rank-2 tensor) to a scalar whereas the diffusion tensor links the components of a vector (a rank-1 tensor) to a scalar.

[2] In Chap. 12, Kindlmann presents a comprehensive work on tensor invariants including anisotropy indices as well as other invariants.

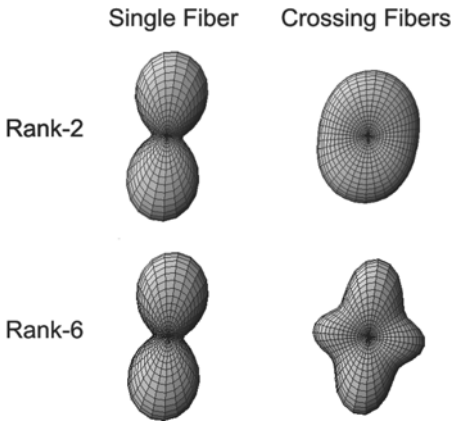

Fig. 10.1. Simulations of the diffusivity profiles from rank-2 (*top*) and rank-6 (*bottom*) tensors from a unidirectional voxel (*left*) and a voxel with two different fiber orientations (*right*). See colour plates

to an excessive smoothing of the diffusivity profile, hence a reduction in the anisotropy value [8]. In Fig. 10.1, we show the diffusivity profiles as implied by rank-2 and rank-6 tensors for simulated unidirectional and directionally heterogeneous voxels. It is clear that employment of a rank-2 tensor gives rise to a significant change in the diffusivity profiles in the presence of multiple orientations. As a result, one may expect inaccurate anisotropy values in such voxels if a rank-2 tensor model is used.

10.2.1 Generalization of Trace

The most widely used indices such as Fractional Anisotropy (FA) and Relative Anisotropy (RA) [9] are not readily generalizable to accomodate diffusivity profiles that are more general than those that can be generated by rank-2 tensors. Therefore, we attempt to express these indices in a way that may make it feasible to generalize them to higher rank tensors as well as to arbitrary functions defined on the surface of a unit sphere. We note that FA and RA can be expressed in terms of the trace of the square of a matrix $\mathsf{R} := \mathsf{D}/\mathrm{trace}(\mathsf{D})$ as

$$\mathrm{FA} = \sqrt{\frac{1}{2}\left(3 - \frac{1}{\mathrm{trace}(\mathsf{R}^2)}\right)}, \text{ and } \mathrm{RA} = \sqrt{3\,\mathrm{trace}(\mathsf{R}^2) - 1}\ . \tag{10.13}$$

The trace of a rank-2 tensor can be expressed as the integral of the quadratic forms of the tensor given by

$$\mathrm{trace}(\mathsf{D}) = \frac{3}{2\pi}\int_{\Omega} \mathbf{g}^{\mathrm{T}}\mathsf{D}\mathbf{g}\,\mathrm{d}\mathbf{g}\ , \tag{10.14}$$

where Ω is the unit hemisphere. Note that this expression can be generalized to functions whose domains are the unit hemisphere because $\mathbf{g}^{\mathrm{T}}\mathsf{D}\mathbf{g}$ is a function on Ω. We will denote this generalized trace operation with 'gentr'. For functions $f(\mathbf{g})$, with antipodal symmetry on the unit sphere, this operation is given by

$$\mathrm{gentr}(f(\mathbf{g})) = \frac{3}{2\pi}\int_{\Omega} f(\mathbf{g})\,\mathrm{d}\mathbf{g} \ . \tag{10.15}$$

Insertion of (10.7) into the above expression enables one to calculate the generalized trace of a rank-l tensor. We have shown that the generalized trace of a rank-l diffusion tensor is independent of the tensor rank and is just 3 times the mean diffusivity value [8].

10.2.2 Anisotropy in Terms of Variance

In this work, we formulate anisotropy in terms of the variance of the normalized diffusivity profile where normalization is achieved (in analogy with the definition of R above) via the expression

$$D_{\mathrm{N}}(\mathbf{g}) = \frac{D(\mathbf{g})}{\mathrm{gentr}(D(\mathbf{g}))} \ . \tag{10.16}$$

Next, instead of $\mathrm{trace}(\mathsf{R}^2)$, we propose to use the quantity $\mathrm{gentr}(D_{\mathrm{N}}(\mathbf{g})^2)$. When a rank-$l$ tensor model is used, this quantity can be shown to be given by

$$\begin{aligned}\mathrm{gentr}(D_{\mathrm{N}}(\mathbf{g})^2) = \ & \frac{1}{6\pi\langle D\rangle^2}\sum_{k_1=1}^{N_{\mathrm{l}}}\sum_{k_2=1}^{N_{\mathrm{l}}}\mu_{\mathrm{k}_1}\mu_{\mathrm{k}_2}D_{\mathrm{k}_1}D_{\mathrm{k}_2} \\ & \times\left(\int_{\Omega}\mathrm{d}\mathbf{g}\prod_{\mathrm{p}_1=1}^{\mathrm{l}}\prod_{\mathrm{p}_2=1}^{\mathrm{l}}g_{\mathrm{k}_1(\mathrm{p}_1)}g_{\mathrm{k}_2(\mathrm{p}_2)}\right) \ ,\end{aligned} \tag{10.17}$$

where mean diffusivity, $\langle D\rangle$, is just

$$\langle D\rangle = \frac{1}{2\pi}\sum_{\mathrm{i}_1=1}^{3}\sum_{\mathrm{i}_2=1}^{3}\cdots\sum_{\mathrm{i}_{\mathrm{l}}=1}^{3}D_{\mathrm{i}_1\mathrm{i}_2\ldots\mathrm{i}_{\mathrm{l}}}\int_{\Omega}g_{\mathrm{i}_1}g_{\mathrm{i}_2}\cdots g_{\mathrm{i}_{\mathrm{l}}}\,\mathrm{d}\mathbf{g} \ . \tag{10.18}$$

Note that the integrals in (10.17 and 10.18) can be evaluated analytically.

It is straightforward to show that the variance of the normalized diffusivities is related to $\mathrm{gentr}(D_N(\mathbf{g})^2)$ through the relationship

$$V := \mathrm{variance}(D_{\mathrm{N}}(\mathbf{g})) = \frac{1}{3}\left(\mathrm{gentr}(D_{\mathrm{N}}(\mathbf{g})^2) - \frac{1}{3}\right) \ . \tag{10.19}$$

This variance value takes its minimum value of 0 only when diffusivities along all directions are equal. This value is independent of l, i.e., the minimum value is the same for all tensor models. This is in contrast with the

supremum value, which is achieved when the diffusivity profile is expressed as proportional to the outer product of same l vectors given by

$$D_{\mathrm{i}_1\mathrm{i}_2\ldots\mathrm{i}_l} = D\, g'_{\mathrm{i}_1} g'_{\mathrm{i}_2} \ldots g'_{\mathrm{i}_l} \quad . \tag{10.20}$$

The variance value associated with this tensor is

$$\text{sup variance}(D_{\mathrm{N}}(\mathbf{g})) = \frac{l^2}{9(2l+1)} \quad . \tag{10.21}$$

In (10.20), $\mathbf{g}'$ is the unit vector specifying the direction of greatest diffusion coefficient and D is this maximal diffusivity. The form of the supremum value in (10.21) implies that

- the supremum value depends on the rank of the model
- there is a limit to the anisotropy of the profiles that can be characterized by lower rank tensor models
- when an arbitrary function is given[3] this supremum value is ∞.

As a result of the last of these findings, a general anisotropy index can be defined as a monotonic function that maps the interval $[0, \infty)$ to $[0, 1)$. Based on this, we define the generalized anisotropy index as

$$\mathrm{GA} := 1 - \frac{1}{1 + (250\mathrm{V})^{\varepsilon(V)}} \, , \tag{10.22}$$

where

$$\varepsilon(V) := 1 + \frac{1}{1 + 5000V} \quad . \tag{10.23}$$

The particular form of this index differs from those of FA and RA in that FA and RA emphasize the variations among pixels with very low anisotropy values. However, the sensitivity of the GA images to changes in variance values is suppressed when those variance values are very small. As a result, the formulation of GA index as given in (10.22–10.23) ensure that the emphasized variations in the variance values are within a window that is more consistent with the variance values observed in the real datasets, increasing the contrast of the anisotropy images.

In Fig. 10.2, we show the GA images implied by rank-2 and rank-6 tensors where the sample is an excised rat brain acquired at 17.6T. Also included are the difference maps demonstrating how much the variance and GA values calculated from rank-6 tensors differ from those calculated from rank-2 tensors. Complicated architecture of the brain stem is distinguished as the bright pixels in the difference maps.

[3] Note that in this case the required tensor model is ∞.

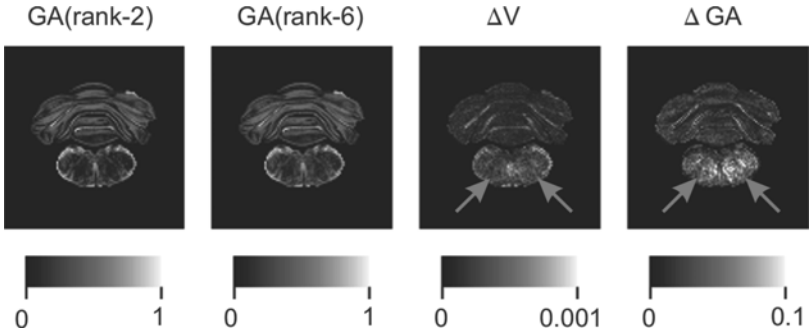

Fig. 10.2. GA values from rank-2 (left column) and rank-6 (second column) tensors from a coronal slice of an excised rat brain image. The right two columns show the difference between the variance and GA values when these two tensor models were used (see colour plates)

10.3 Fiber Orientations Implied by Higher Rank Tensors

The underlying hypothesis in the utilization of diffusion weighted imaging to map fiber orientations in tissue is that the major orientations along which diffusion occurs coincide with the fiber orientations. Therefore, in order for one to have a correct orientation map, he needs to accurately estimate a function $\overline{P}(\mathbf{x}, t_\mathrm{d})$ that is just the probability of water molecules to move a distance $\mathbf{x}$ during a time t_d. It is known from q-space imaging [10] that the average of this function over the voxel is just the Fourier transform of the signal attenuations (assuming $\delta << \Delta$), where the signal is envisioned to be on the reciprocal space of $\mathbf{x}$ defined by the gradient directions:

$$\overline{P}(\mathbf{x}, t_\mathrm{d}) = \int \mathrm{d}\mathbf{q}\, \frac{S(\mathbf{q})}{S_0}\, \exp(-i2\pi\mathbf{q}\cdot\mathbf{x})\,, \tag{10.24}$$

where $\mathbf{q} := (2\pi)^{-1}\gamma\delta G\mathbf{g}$.

Note that in the rank-2 tensor model of traditional DTI, making the substitution (from (10.4))

$$\frac{S(\mathbf{q})}{S_0} = \exp\left(-4\pi^2 q^2 t_\mathrm{d}\mathbf{g}^\mathrm{T}\mathsf{D}\mathbf{g}\right) \tag{10.25}$$

into (10.24) results in the well-known oriented Gaussian displacement profile for water molecules

$$\overline{P}(\mathbf{x}, t_\mathrm{d}) = \frac{1}{\sqrt{(4\pi t_\mathrm{d})^3 \det(\mathsf{D})}}\, \exp\left(\frac{-\mathbf{x}^\mathrm{T}\mathsf{D}^{-1}\mathbf{x}}{4t_\mathrm{d}}\right)\,. \tag{10.26}$$

Although (10.25) is known to be incorrect for large values of $\mathbf{q}$, DTI has been found to be quite successful in the determination of fiber directions when the voxel of interest is unidirectional.

In the case of rank-2 DTI, in order to find the fiber direction, it is sufficient to diagonalize the diffusion tensor because the peak of the displacement and diffusivity profiles coincide and are given by the principal eigenvector of the diffusion tensor.

In this work, we generalize these ideas to the case when diffusion is characterized by a tensor of rank possibly higher than 2. Following the same lines with the above formulation, we make the same monoexponentiality assumption as in (10.25), and write

$$\frac{S(\mathbf{q})}{S_0} = \exp\left(-4\pi^2 q^2 t_{\mathrm{d}} D(\mathbf{g})\right) \ , \tag{10.27}$$

where in the case of a rank-l tensor model, $D(\mathbf{g})$ will be given by (10.7). It is a formidable task to analytically calculate the $\overline{P}(\mathbf{x}, t_{\mathrm{d}})$ function corresponding to a rank-l tensor model. Therefore, we adopt a numerical scheme in which we sample the q-space on a rectangular regular lattice using (10.27). We use a $64 \times 64 \times 64$ grid such that the largest q-value corresponds to a b-value of 60000 s/mm^2. Then we apply the FFT algorithm to estimate the displacement probabilities [11].

In Fig. 10.3, we show the simulations of 1, 2 and 3 fiber systems. Clearly rank-2 DTI fails to give meaningful results when there are more than one fiber directions. As seen in the third column, the peaks of the diffusivity profiles do not correspond to the fiber orientations when there are more than one fiber orientation. Increasing the rank of the tensor model however, enables the visualization of the different fiber bundles. In the last column, we apply a sharpening transformation to the isosurfaces of the displacement probability

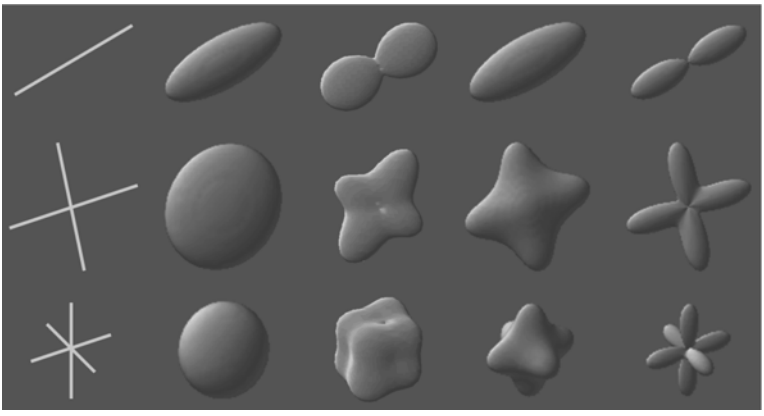

Fig. 10.3. The simulation results (see colour plates). The three rows show the 1, 2 and 3 fiber systems from top to bottom. The different columns show the orientations of the cylinders, probability isosurfaces obtained using rank-2 DTI, diffusivity profiles, equiprobability surfaces from rank-6 DTI, and these probability surfaces after a sharpening transformation (from *left* to *right*)

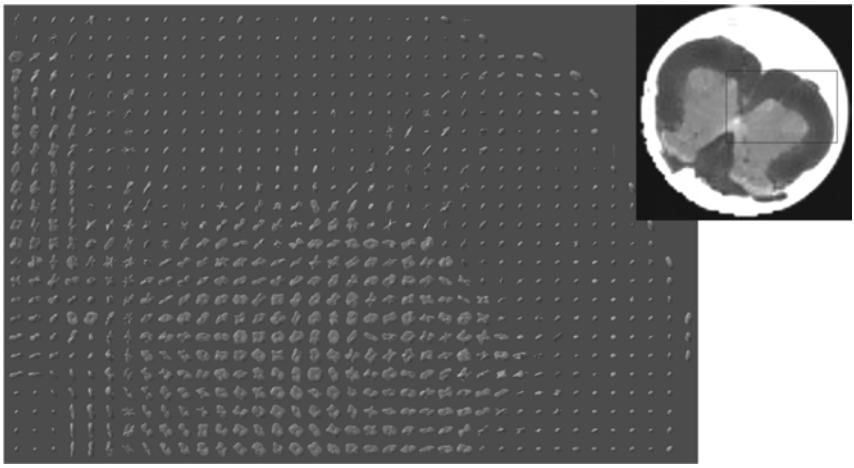

Fig. 10.4. Isosurfaces of displacement probability functions implied by a rank-6 tensor model from a selected region of interest (ROI) in an excised rat spinal cord image. The top right image is from a non-diffusion weighted dataset showing the ROI where the probability isosurfaces were calculated (see colour plates)

profile that involves the removal of the largest sphere that fits into the surface. This step can be thought of as an operation analogous to disregarding of the smaller eigenvalues of the diffusion tensor in traditional DTI.

Figure 10.4 shows the sharpened isosurfaces of the displacement profiles calculated on a slice of excised rat spinal cord imaged at 14.1 T. The rank of the tensor model employed was 6. Fiber crossings are visible in many areas in the spinal cord, particularly in the ventral nerve roots that travel among white-matter fiber bundles in a direction perpendicular to them and causing partial volume effects. Also note the complicated structure in gray-matter where most fibers are oriented in the plane of the image.

Acknowledgments

We would like to acknowledge Dr. Tim M. Shepherd of Neuroscience department for useful discussions. This work was supported by National Institutes of Health grant numbers P41-RR16105 and R01-NS42075. The magnetic resonance images were acquired in the Advanced Magnetic Resonance Imaging and Spectroscopy Facility of the McKnight Brain Institute. The experiments on animal tissue were performed with the approval of the University of Florida Institutional Animal Care and Use Committee.

References

1. Basser P. J., Mattiello J., et al. (1994) MR diffusion tensor spectroscopy and imaging. Biophys. J. **66** (1), 259–267.
2. Basser P. J., Mattiello J., et al. (1994) Estimation of the effective self-diffusion tensor from the NMR spin echo. J. Magn. Reson. B **103**(3), 247–254.
3. Torrey H. C. (1956) Bloch equations with diffusion terms. Phys. Rev. **104**(3), 563–565.
4. Stejskal E. O., Tanner J. E. (1965) Spin diffusion measurements: Spin echoes in the presence of a time-dependent field gradient. J. Chem. Phys. **42**(1), 288–292.
5. Özarslan E., Mareci T. H. (2003) Generalized diffusion tensor imaging and analytical relationships between diffusion tensor imaging and high angular resolution diffusion imaging. Magn. Reson. Med. **50**, 955–965.
6. Schouten J. A. (1989) Tensor Analysis for Physicists. New York Dover Publications.
7. Dong Q., Welsh R. C., et al. (2004) Clinical applications of diffusion tensor imaging. J. Magn. Reson. Imaging **19**(1), 6–18.
8. Özarslan E., Vemuri B. C., et al. (2004) Generalized scalar measures for diffusion MRI using trace, variance and entropy. Magn. Reson. Med., *accepted.*
9. Basser P. J. (1995) Inferring microstructural features and the physiological state of tissues from diffusion–weighted images. NMR Biomed. **8**, 333–344.
10. Callaghan P. T. (1991) Principles of Nuclear Magnetic Resonance Microscopy. Oxford Clarendon Press.
11. Özarslan E., Vemuri B. C., et al. (2004) Multiple fiber orientations resolved by generalized diffusion tensor imaging. Proc. Intl. Soc. Mag. Reson. Med. 89.